University of Plymouth

PEARL **https://pearl.plymouth.ac.uk**

Faculty of Science and Engineering School of Biological and Marine Sciences

2013-09

Generation of baroclinic tides over an isolated underwater bank

Vlasenko, Vasyl

http://hdl.handle.net/10026.1/3843

10.1002/jgrc.20304
Journal of Geophysical Research: Oceans
American Geophysical Union (AGU)

All content in PEARL is protected by copyright law. Author manuscripts are made available in accordance with publisher policies. Please cite only the published version using the details provided on the item record or document. In the absence of an open licence (e.g. Creative Commons), permissions for further reuse of content should be sought from the publisher or author.

JOURNAL OF GEOPHYSICAL RESEARCH: OCEANS, VOL. 118, 1–14, doi:10.1002/jgrc.20304, 2013

Generation of baroclinic tides over an isolated underwater bank

Vasiliy Vlasenko,[1] Nataliya Stashchuk,[1] Matthew R. Palmer,[2] and Mark E. Inall[3]

Received 1 March 2013; revised 31 May 2013; accepted 3 July 2013.

[1] The interaction of stratified tidal flow with an isolated bank (Jones Bank in the Celtic Sea) was investigated numerically and using observational data collected during the 25th research cruise of the R/V *James Cook* in July 2008. Two scenarios of observed wave generation, one with pure tidal forcing and another with an extra background current, were reproduced numerically and compared against the observational data. It was found that the tidal currents alone produced subcritical conditions for the first-mode internal wave generation and supercritical flow for the second-mode waves. Under these conditions, the first-mode waves with amplitudes up to 10 m freely radiated from the bank, gradually transforming into attenuating dissipative baroclinic bores. Due to supercritical conditions, the second-mode waves were arrested at the lee side of the bank for 3 h where they grew in amplitude (up to 35 m) and after their release propagated as a series of second-mode internal solitary waves. The additional background current that was measured near the bank in the middle of June 2008 radically changed the conditions of wave generation. A strong southeastern current arrested the first-mode perturbations at the NE flank of the bank for 2 h, where they grew in amplitude to almost 40 m and disintegrated into packets of first-mode internal solitary waves after their release. For the second-mode perturbations, the flow was substantially supercritical for more than one fourth of a tidal period so that these waves were just washed away from the generation site without any visible amplification.

Citation: Vlasenko, V., N. Stashchuk, M. R. Palmer, and M. E. Inall (2013), Generation of baroclinic tides over an isolated underwater bank, *J. Geophys. Res. Oceans*, *118*, doi:10.1002/jgrc.20304.

1. Introduction

[2] One of the principal mechanisms that provides the majority of the turbulent kinetic energy production in the ocean at a level sufficient for keeping the stability of oceanic stratification is the interaction of a stratified tidal flow with the bottom topographies. To date, most in situ studies have been focused on the investigation of internal waves that were generated by tides near continental slopes and oceanic ridges [see *Garrett and Kunze*, 2007, and references therein]. Much less attention has been paid to the internal waves that had their origin at localized topographic features.

[3] *Carter et al*. [2006] reported observations of tidal flow and mixing around a small seamount on Kaena Ridge (Hawaii). Here strong tidal energy conversion from barotropic to baroclinic components was found over Kaena Ridge with a remarkable asymmetry of the internal wavefield in space and a relatively weak contribution of the seamount into the total energy budget due to its small height. Another tidal flow investigation was made in the shallow water of Georges Bank by *Brickman and Loeder* [1993]. They concluded that hydraulic jumps which were generated over the bank during each tidal cycle controlled the characteristics of radiated internal waves and associated mixing. Similar investigations near the shallow 30 m Stellwagen Bank (the total shelf depth 90 m) were conducted by *Hibiya* [1988], and in the area of Stonewall Bank by *Moum and Nash* [2000] [see also *Nash and Moum*, 2001]. It was confirmed in each case that supercritical tidal flow over shallow water banks produced hydraulic jumps, which resulted in significantly enhanced internal mixing. Similar results were obtained also for deep water topographies; see observations reported by *Klymak et al*. [2008] for Kaena Ridge. Most recently the effect of supercritical tidal topographies on internal tidal mixing was quantified by *Klymak et al*. [2010].

[4] Unlike two-dimensional (2-D) configurations such as Knight Inlet in British Columbia, where the place of generation of internal lee waves is well predicted [see *Farmer and Armi*, 1999] and the experimental methodology can be adjusted accordingly, an accurate experimental record and quantification of the lee waves that are generated near three-dimensional (3-D) features is a more challenging task. In the case of real 3-D topographies, the areas of hydraulic control can be spatially restricted. Being released from these local sources, the lee waves are radiated as circular patterns and attenuate quickly due to radial divergence. The difficulties in observational detection of the lee waves at a bank to the east of Race Rocks (coastal area of

[1]School of Marine Science and Engineering, Plymouth University, Plymouth, UK.
[2]National Oceanographic Centre, Liverpool, UK.
[3]Scottish Association for Marine Science, Oban, UK.

Corresponding author: V. Vlasenko, School of Marine Science and Engineering, Plymouth University, Plymouth PL4 8AA, UK. (vvlasenko@plymouth.ac.uk)

©2013. American Geophysical Union. All Rights Reserved.
2169-9275/13/10.1002/jgrc.20304

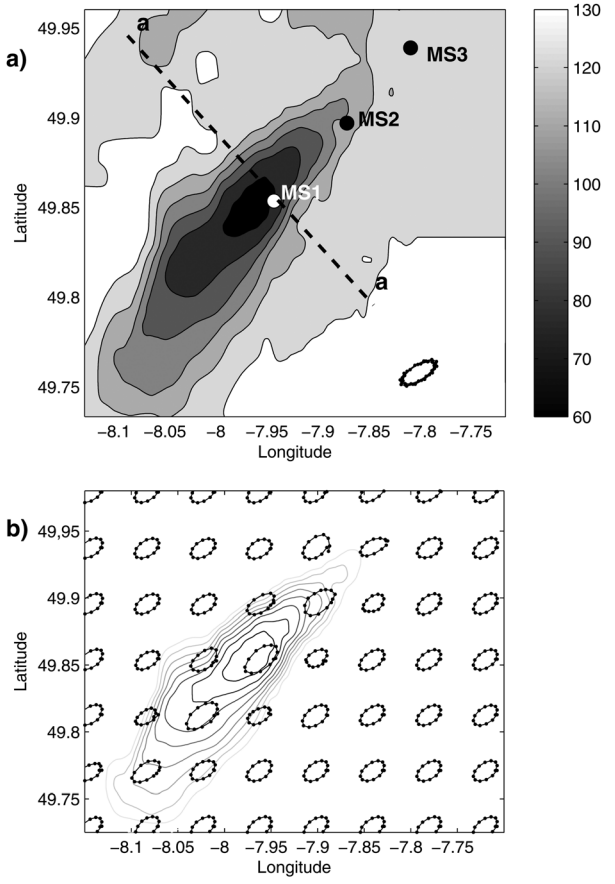

Figure 1. (a) Bathymetry of Jones Bank with the positions of three moorings, MS1, MS2, and MS3, deployed in the cruise. (b) Tidal ellipses reproduced by the MITgcm in the area. For the comparison reason, the TPXO7.1-predicted tidal ellipse for the point MS2 is shown at the right bottom corner of Figure 1a.

Vancouver Island, British Columbia) was reported by *Dewey et al*. [2005]. Within one tidal cycle, the Froude number in the area varied in a range from subcritical to supercritical values. The conditions of hydraulic control were detected at only one of the moored acoustic Doppler current profilers (ADCPs). All other moorings deployed in the area and a ship-mounted ADCP did not reveal evidence of the lee waves, although backscatter satellite imagery consistently showed that internal wave packets radiated from the bank on every tidal cycle. It was concluded that more accurate experimental planning is required for tracking the lee waves during their generation, evolution, and dissipation.

[5] The most recent in situ observations of the lee-wave mechanism of internal wave generation near a small-scale bank were conducted by *Palmer et al*. [2013] in the area of Jones Bank (the Celtic Sea). Three moorings equipped with up-looking bottom-mounted ADCPs and thermistor chains were deployed in the area (Figure 1a). The supercritical regime that results in the generation of internal lee waves was confirmed by *Palmer et al*. [2013]. They used the data collected by the mooring deployed at the bank's top, although a detailed analysis of the characteristics of the generated waves has not been conducted because the collected data set was not complete enough to quantify all the spatial and temporal characteristics of the generated waves.

[6] In general, comprehensive theoretical studies of baroclinic tides generated near isolated 3-D topography features are presently lacking. To date, most model investigations have been focused on internal tides produced by 2-D topographies, and for decades much attention was directed to the study of the generation from shelf-slope areas [*Garrett and Kunze*, 2007]. A relatively small number of numerical studies have focused on topographic generation of baroclinic tides near isolated 3-D seamounts. *Holloway and Merrifield* [1999] and later *Munroe and Lamb* [2005] investigated the wave generation by tidal flow over 3-D Gaussian bumps. It was found that one of the basic parameters that controls the intensity of generated fields is the horizontal aspect ratio (the longest to the shortest horizontal length scales of the topography). The generation of internal waves would be ineffective unless the major axis of the elongated seamount was perpendicular to the barotropic flow. Both investigations were conducted using the hydrostatic Princeton Oceanographic Model (POM) with quite a coarse resolution and low forcing intensity which did not allow for investigation of strong nonlinear and nonhydrostatic effects like internal solitary waves that are common features for oceanic conditions. Similarly, no strongly nonlinear wave effects were investigated by *Johnston and Merrifield* [2003], who studied scattering of internal tidal waves by 3-D seamounts using a hydrostatic POM.

[7] The requirements for a successful model replication of the lee-wave mechanism of generation of internal waves near localized bottom topographies are as follows:

[8] (1) An accurate, fine-resolution 3-D bottom topography

[9] (2) Realistic stratification, taken from observations

[10] (3) Correct setting of tidal forcing

[11] (4) Inclusion of full nonlinearity and nonhydrostaticity into the numeric code

[12] All of these requirements are essential to get an acceptable level of consistency between 3-D observations and modeling. The fully nonlinear nonhydrostatic Massachusetts Institute of Technology general circulation model (MITgcm) [*Marshall et al*., 1997] was applied to study the highly nonlinear internal lee waves generated in the area of Jones Bank. The model output was validated against the observational data collected in the 25th cruise of the R/V *James Cook* in July 2008 [*Palmer et al*., 2013].

[13] This paper is organized as follows. Section 2 discusses the details of the field experiments. Section 3 briefly outlines the model setup. All of the basic model results are discussed in section 4, and conclusions are formulated in section 5.

2. Experimental Data

[14] An investigation of mixing process in the Celtic Sea was conducted on the 25th cruise of the R/V *James Cook* in July 2008 (hereafter JC25) in the area of Jones Bank, which is an isolated topographic feature located in the central part of the Celtic Sea over 200 km east of the shelf break [*Inall et al*., 2011]. The bank is elongated in the southwest-northeast direction over 50 km along its main axis and rises over 60 m from an average 130 m depth of the surrounding areas (Figure 1a).

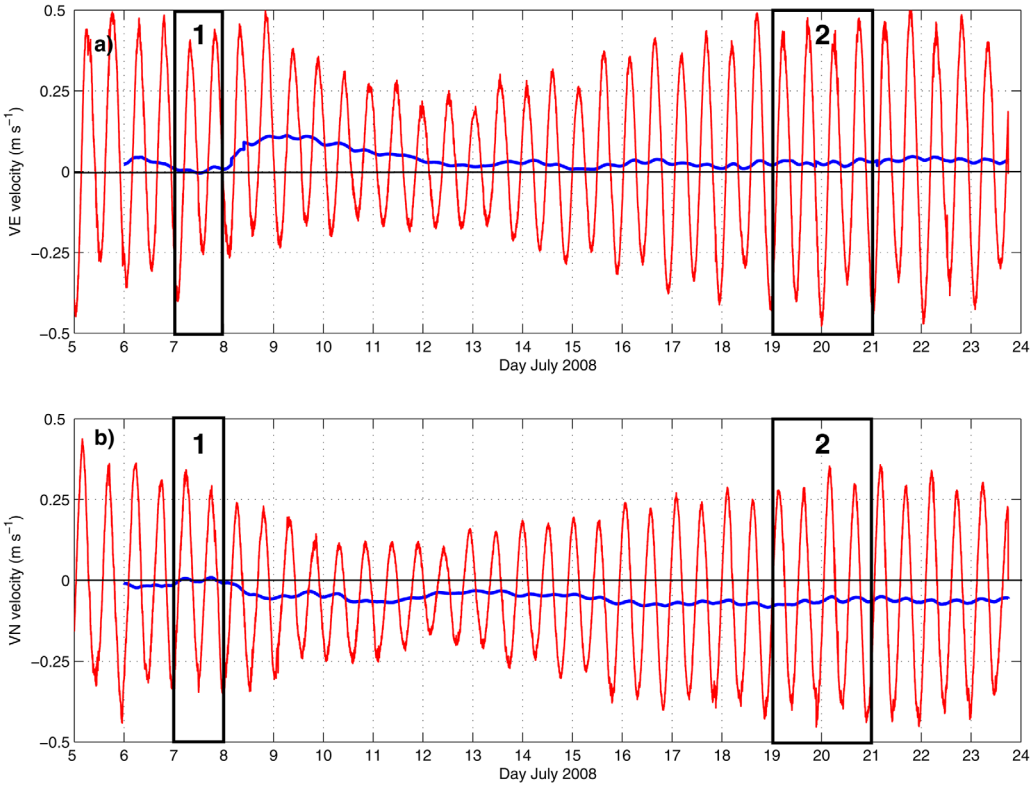

Figure 2. (a) Zonal and (b) meridional vertically averaged velocities recorded at mooring MS1. Blue lines show residual currents. Black rectangles 1 and 2 correspond to two observational time intervals reproduced in the paper.

[15] The mission of JC25 was an investigation of stratified tidal flow around the bank and its influence on the spatial and temporal characteristics of mixing processes developing in the area [*Palmer et al*., 2013]. For this purpose, three moorings, MS1, MS2, and MS3, were deployed near the bank as shown in Figure 1a: MS1 (49°51.21′N; 07°56.87′W), MS2 (49°53.82′N; 07°52.58′W), and MS3 (49°56.33′N; 07°48.83′W). Each mooring was equipped with a bedframe-mounted RDI 300 kHz ADCP, which recorded along-beam velocities with 1 s temporal and 2 m spatial resolutions that were recalculated into horizontal velocities [*Palmer et al*., 2013]. A vertical chain of thermistors at each station recorded temperature every minute with 2 m vertical resolution in the upper half of the water column and 5 m near the bottom. Unfortunately, the ADCPs at MS2 and MS3 failed to work after 12 July 2008, but the ADCP at MS1 successfully recorded velocity data for the entire deployment period from 5 July to 24 July 2008.

[16] The meridional and zonal components of the barotropic tidal velocity (vertically averaged ADCP records) for mooring MS1 are shown in Figure 2. These time series clearly reveal the predominance of M2 semidiurnal tidal harmonics with a more than twofold neap-spring variability of barotropic tidal activity. Low pass 25 h running average filtering of the depth-averaged currents at MS1 revealed residual current shown by solid blue lines in Figure 2. It is evident that at the start of measurements, on 5–8 July 2008, there were no strong stationary currents in the area. However, as seen in Figure 2, a stationary current slowly developed during the next 3 weeks. The zonal component of the current increased from zero to 0.05 m s^{-1} by the middle of July 2008 and was accompanied by a gradual increase of the meridional component (up to 0.03 m s^{-1}).

3. Numerical Model

[17] The hydrodynamics of Jones Bank were modeled using the MITgcm code [*Marshall et al*., 1997]. The numerical experiments were conducted on a fine-resolution grid with the horizontal step of 50 m in meridional and zonal directions. Beyond the central part of the model domain shown in Figure 1, some extra lateral areas were added with increment of grid step from 50 m to 50 km. Such a telescopic increase of the horizontal step prevents reflection of waves from the model boundaries during at least 10 tidal periods and provides an accurate solution without pollution by reflected signals. The vertical model step Δz was also variable, changing from 5 m in the upper 40 m surface layer, below which Δz was increased to 10 m.

[18] Tidal forcing was initialized in the model by setting some extra periodical terms in the right-hand side (RHS) of the momentum balance equations. The tidal ellipses reproduced by the model in a homogeneous fluid were compared against the predictions of the global inverse tidal model TPXO 7.1 [*Egbert and Erofeeva*, 2002]; for 7 July 2008, the tidal ellipse is shown in Figure 1a. The easterly and northerly components of the external pressure gradients and the phase shift between them in the momentum balance equations have been chosen in such a way that the

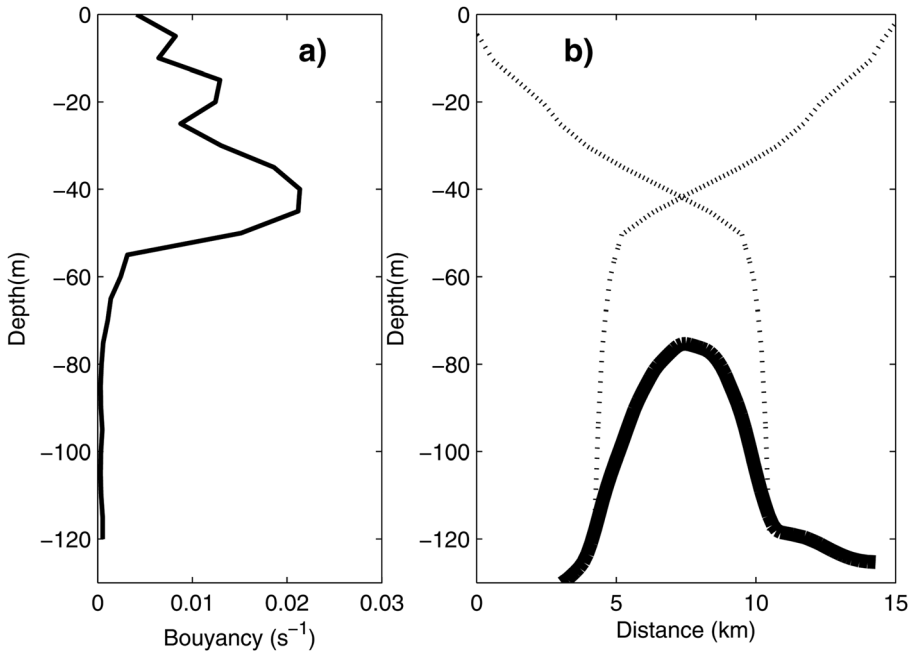

Figure 3. (a) Buoyancy frequency profile used in the initial setup of the model and (b) profile of the bottom topography along the cross-section *a-a* shown in Figure 1a with the M2 tidal wave characteristic lines (shown by dotted lines).

ellipticity parameter of the tidal ellipses and the direction of their major axis coincide with the TPXO predictions. It is clear from Figure 1b that the code reproduces the barotropic tidal flow in the area quite accurately. Both the length of the major and minor semi-axes of the tidal ellipses and their southwest-northeast orientation are almost identical in the two models, which provides confidence in the barotropic forcing for the simulations reported here.

[19] After setting the tidal forcing for a homogeneous fluid, stratification was introduced into the model domain. Fluid stratification was taken directly from conductivity-temperature-depth (CTD) measurements conducted during JC25. The buoyancy frequency profile $N^2(z) = -g/\rho(\delta\rho/\delta z)$ (g is the acceleration due to gravity and ρ is the density) is shown in Figure 3. Appropriate characteristic rays,

$$z = \pm\sqrt{(\omega^2 - f^2)/(N^2(z) - \omega^2)}x + const,$$

of the hyperbolic wave equation for the M2 tidal frequency ω (here f is the Coriolis parameter) are shown in Figure 3b together with the bottom section through line a-a in Figure 1a. Figure 3b shows that the steepness of the characteristic lines is comparable with the inclination of local bottom topography; thus, the generation of baroclinic modes with numbers >1 is expected in the area of Jones Bank [*Vlasenko et al*., 2005].

[20] The large-amplitude internal waves produce strong shear and mixing in close proximity to the place of generation; thus, a Richardson number dependent parameterization for turbulent closure of vertical viscosity ν and diffusivity κ [*Pacanowski and Philander*, 1981] was used:

$$\nu = \frac{\nu_0}{(1+\alpha \mathrm{Ri})^n} + \nu_b, \qquad \kappa = \frac{\nu}{(1+\alpha \mathrm{Ri})} + \kappa_b,$$

where Ri is the Richardson number, $\mathrm{Ri} = N^2(z)/\left(u_z^2 + v_z^2\right)$, u and v are the components of horizontal velocity; $\nu_b = 10^{-5}$ m^2 s^{-1} and $\kappa_b = 10^{-5}$ m^2 s^{-1} are the background viscosity, $\nu_0 = 1.5 \times 10^{-2}$ m^2 s^{-1}; and $\alpha = 5$ and $n = 1$ are the adjustable parameters. Such a parameterization increases ν and κ in areas where the Richardson number is small. The horizontal viscosity and diffusivity were set to a constant value of 0.5 m^2 s^{-1}.

[21] According to the ADCP data shown in Figure 2, the stratified flow around Jones Bank is a superposition of stationary current and tides. To take into account the background current and to study how it can affect the generation of internal waves, two series of numerical experiments were conducted: (i) In the first experiment, the tidal currents were set into the code (corresponding to the time shown by rectangle 1 in Figure 2) and (ii) the second experiment was initialized by the same spring intensity of tidal forcing as for (i) and with an additional 0.05 m s^{-1} southeasterly stationary current (corresponding to the time shown by rectangle 2 in Figure 2). The current was introduced in the code by two extra stationary terms added to the RHS of the momentum balance equations. To avoid the generation of spurious inertial oscillations, the current velocities were increased from zero to a stationary value over 10 h, which is much longer than one fourth of the inertial period (4 h). The tidal currents were initialized in the code after stationary currents stabilized (at least 2 additional days).

4. Numerical Results

4.1. Experiment I: Tidal Forcing

[22] Initial validation of the model data was undertaken using observational data from the field campaign collected

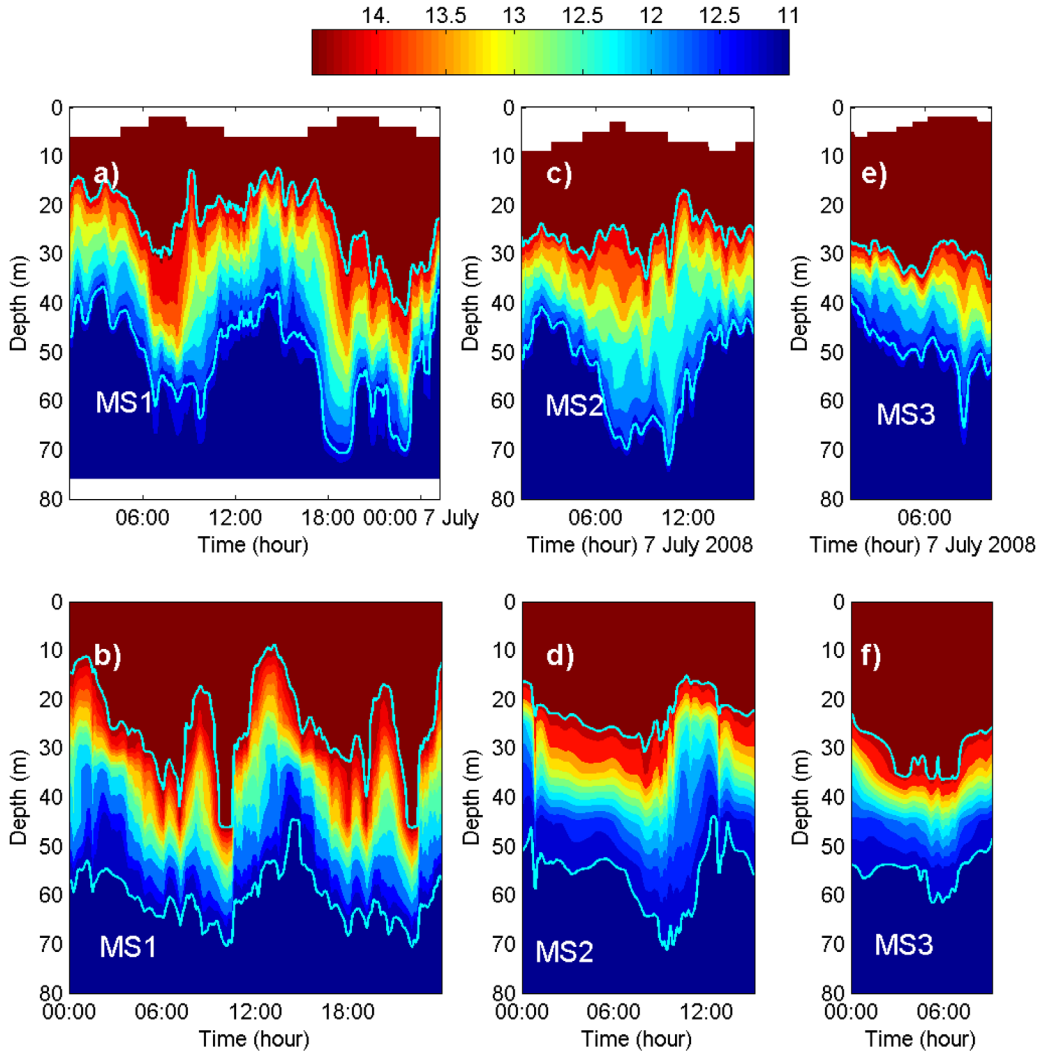

Figure 4. (top) Temperature recorded at moorings (a) MS1, (c) MS2, and (e) MS3 on 7 July 2008 when no background current was observed. (bottom) Model-predicted temperature for moorings (b) MS1, (d) MS2, and (f) MS3. Positions of moorings are depicted in Figure 1.

on the 7 July 2008 (Figure 2) and model data forced only by tidal currents.

[23] Figure 4 presents the time series of temperature recorded at moorings MS1, MS2, and MS3 (see Figure 1a) during the field experiment on 7 July 2008 (Figures 4a, 4c, and 4e) when the background current was close to zero (see Figure 2) and model-predicted temperature fields for the very same time periods (Figures 4b, 4d, and 4f). Comparison of modeled and observed data sets at mooring MS1 shows their consistency. The maximum vertical extent of baroclinic oscillations is 40–50 m, which is comparable to the total water depth (80 m at mooring MS1) and testifies to the large contribution of nonlinear effects that can develop near the bank.

[24] The possibility of generation of high baroclinic modes by tides near Jones Bank was discussed earlier on the basis of the analysis of the background stratification and bottom topography (Figure 3). The second baroclinic mode is clearly evident, recognizable as a sudden widening and narrowing of the thermocline in Figures 4a and 4b.

[25] Time series of temperature at two other moorings, i.e., MS2 and MS3 (Figures 4c–4f), also reveal a similarity between the model outputs and the observations (general structure and vertical amplitudes), although the coincidence is not as obvious as it was for MS1. One explanation could be the presence of other waves generated remotely from Jones Bank.

[26] The spatial structure of the internal wavefield was investigated by using the value of the gradient of horizontal velocity $Gr = \sqrt{u_x^2 + v_y^2}$ at the free surface [*Stashchuk and Vlasenko*, 2005]. A similar routine is usually applied for the detection of strongly nonlinear internal waves in comparison with synthetic aperture radar satellite images. The model data were considered after 3.5 tidal cycles, when all transitional processes developed during the model spin-up have already been attenuated. Figure 5 shows surface signals produced by internal waves at four different moments of time (with a 3 h time interval). It is seen that the wavefield consists of a number of locally generated and spatially restricted wave packets radiated from Jones Bank. Bearing

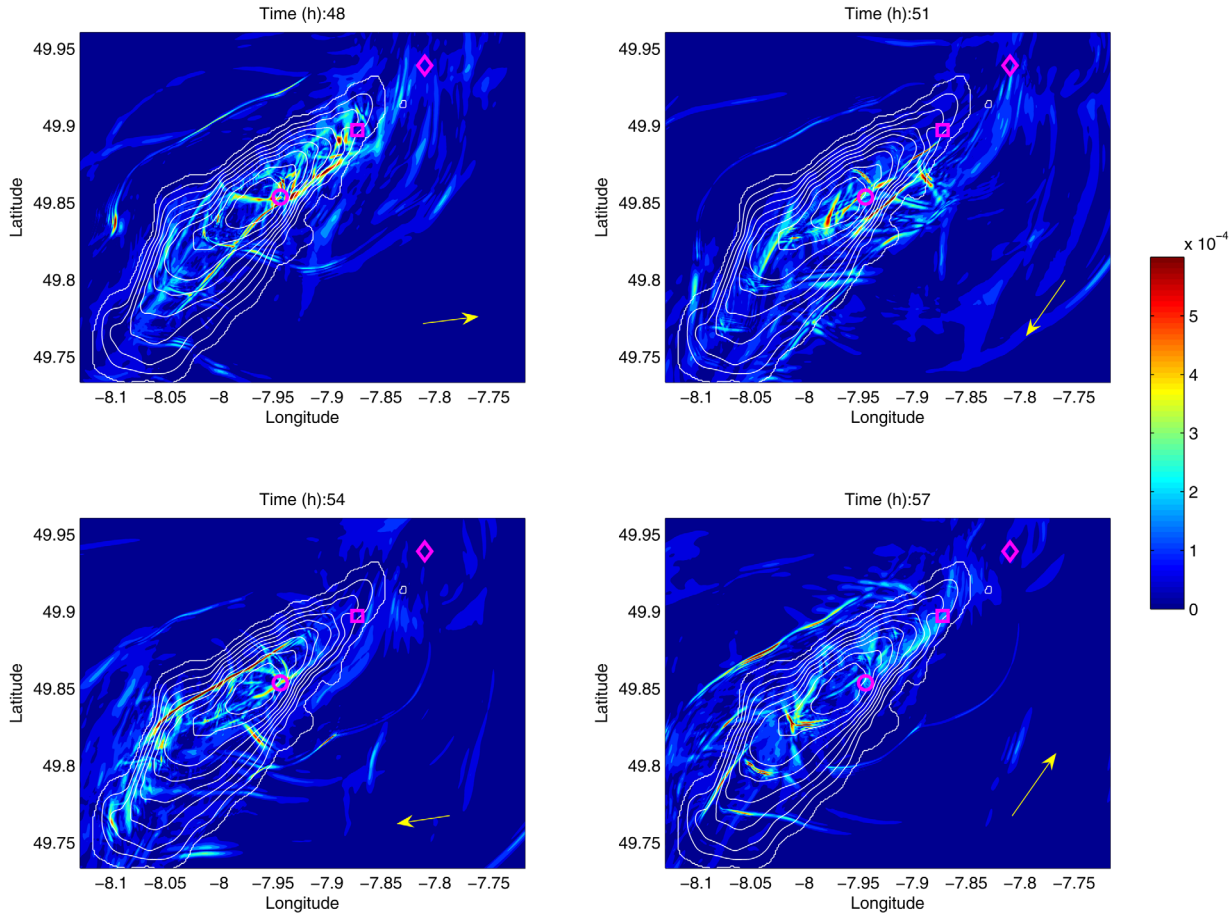

Figure 5. Gradients of horizontal velocity Gr (in s^{-1}) on the free surface (light blue and yellow-red colors) at different stages of tidal cycle showing evolution of internal waves radiated from Jones Bank. Yellow arrows show the direction of the tidal current. Positions of moorings are shown by red symbols.

in mind this diversity, it would be very difficult to describe every single wave in full detail during its evolution over one tidal cycle. Instead, we will focus on the comprehensive analysis of only the strongest wave systems that carry away the major part of the wave energy.

[27] Figure 6a represents overlaid signatures for one tidal cycle of the two strongest wave systems with horizontal velocity gradients more than 3×10^{-4} s^{-1} (marked by red and blue colors). The waves that were apparent for <3 h were omitted from analysis. The signatures of the third wave front shown in green in Figure 6a are less energetic ($Gr < 2.5 \times 10^{-4}$ s^{-1}) and are used here for the comparison with the first two waves. The positions of three waves are given with a 1 h temporal step to trace the place of their generation and their position during evolution. The numbers that accompany each wave signature correspond to the hour when it was detected. The direction of propagation of all three waves is shown by the dashed lines with arrows in the appropriate color.

[28] To understand the structure of the three waves with the signatures given in Figure 6, density cross-sections perpendicular to the wave fronts (i.e., along the dashed line, Figure 6a) were calculated and are presented in Figure 7. A joint analysis of Figures 6 and 7 can help to understand the horizontal spatial and vertical modal structures of the generated waves. Additionally, the inset in Figure 6a shows the direction of the tidal current vector at different moments in time.

[29] We start our analysis with Wave 1 (red signatures in Figure 6a) that according to Figure 7 at $t \geq 51$ h represents a second-mode wave fragment indicated by diverging isopycnals. In fact, this wave evolved from a lee wave generated at the lee side of the southeastern flank of the bank where it was arrested for ~3 h (from $t = 48$ h to $t = 51$ h; see Figure 6). Interestingly, as distinct from a typical 2-D situation, the arrested lee waves in a 3-D case are not fixed at any particular place. Figure 6 shows that Wave 1 rotates in space adjusting permanently upstream to the rotating tidal flow (compare this to the spatial structure of Wave 1 fronts at $t = 48$–51 h).

[30] By $t = 49$ h, Wave 1 fragment turns to a combination of a first-mode wave of depression (hydraulic jump) with a maximum vertical scope of ~30–35 m that was followed by Wave 1 marked by a varicose widening of the pycnocline (second-mode signature). By the next time step ($t = 51$ h), the first-mode wave is not visible in the cross section because it was radiated from the generation area. When the tide was directed to the west, Wave 1 gradually transformed into a 20 m second-mode baroclinic bore (see plot for $t = 54$ h) and 4 h later disintegrated into a packet of

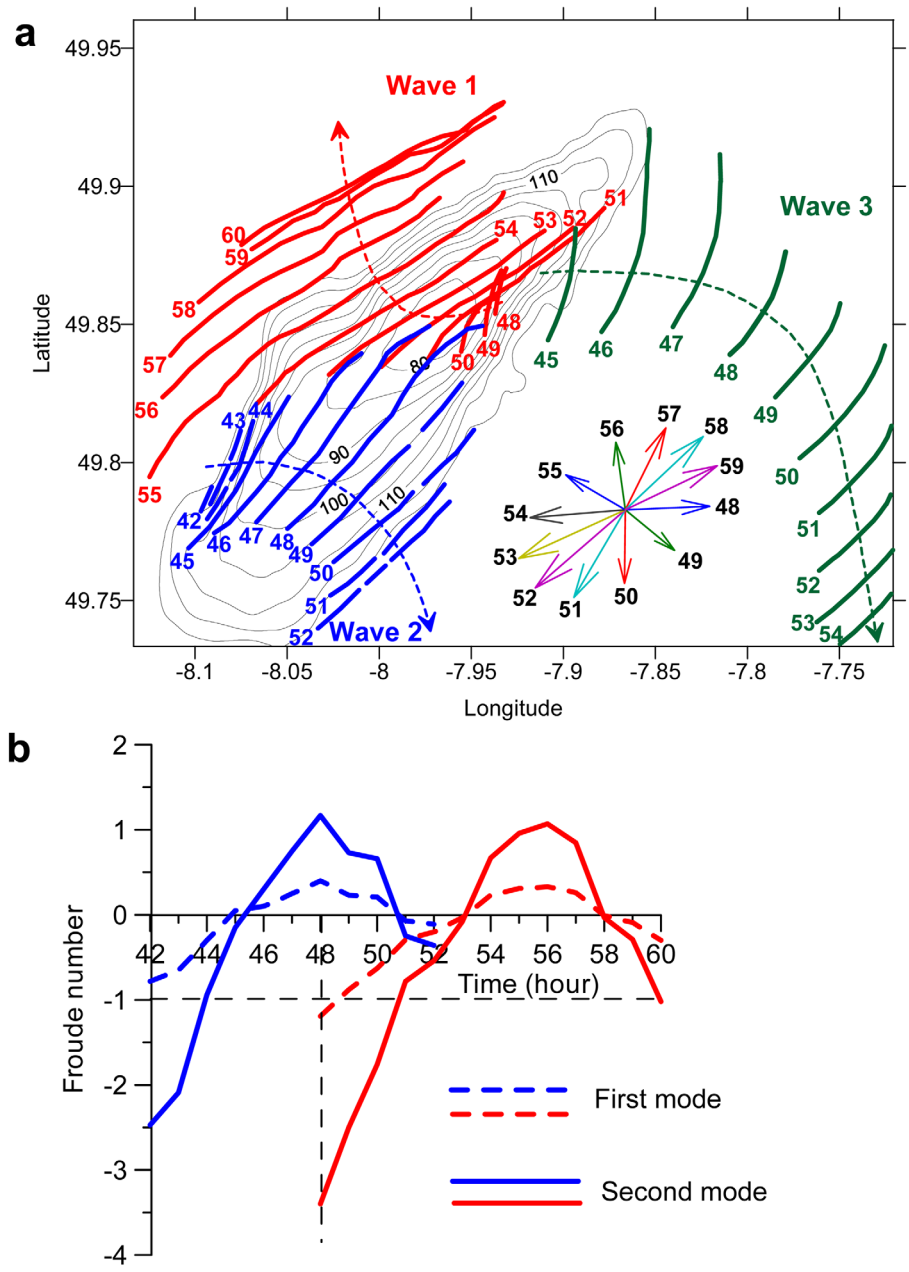

Figure 6. (a) Surface signature of internal waves generated at different moments of tidal cycle. Positions of only the strongest wave packets are presented with 1 h interval. Direction and strength of the tidal currents are shown by a tidal diagram in the bottom right. (b) The Froude number calculated for Waves 1 and 2 in the positions where their centers were at every particular moment of time (along dashed lines). The Froude number for the first mode Wave 3 is the same as shown by the dashed blue line.

second-mode internal solitary waves with amplitudes ~10 m ($t = 58$ h). At the end of the tidal cycle, the wave packet was arrested off the bank by tidal current moving in the opposite direction (compare the wave signature at $t = 59$ h and $t = 60$ h in Figure 6) and was ultimately destroyed.

[31] Wave 2 (blue signatures in Figure 6a) was generated half a cycle earlier than Wave 1 at the opposite side of the bank. It propagated in a SE direction and according to Figure 7 almost identically repeats the dynamics and structure of Wave 1. It was arrested by the tidal current for 2–3 h at the lee side of the bank ("blue" wave fronts for 42–45 h in the left bottom corner of Figure 7) and grew in amplitude as a second-mode baroclinic bore (Figure 7). The vertical scale of Wave 2 was smaller than those of Wave 1, which is why the wave packet contains only one second-mode solitary wave (the most right plot in the middle row of Figure 7).

[32] Wave 3, with the signatures shown by green in Figure 6a, represents a first-mode baroclinic wave. The mechanism of its generation is somewhat different from the

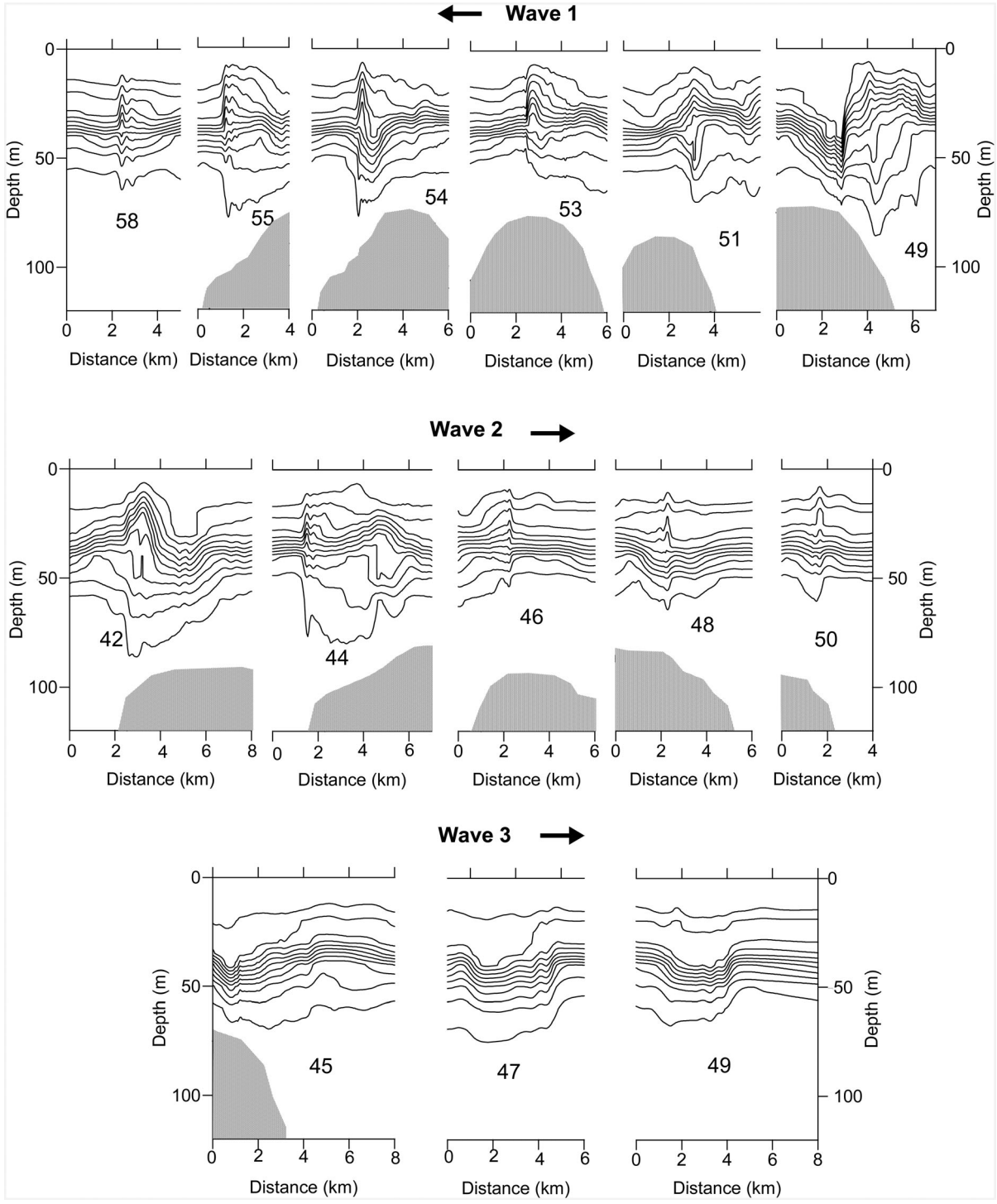

Figure 7. Cross sections of density calculated along the blue, red, and green dashed lines shown in Figure 6a. The line interval is equal to 0.1 kg m^{-3} starting with $\sigma_t = 26.1$ kg m^{-3} at the shallowest isoline. Numbers in the middle of every plot depict the moment of tidal cycle in hours.

lee-wave mechanism discussed above. As seen from Figures 6a and 7, Wave 3 is not arrested by the tidal flow at the lee side of the topography as was the case with Waves 1 and 2. Instead, it is generated locally at the northeastern flank of the bank (see Figure 7) and radiates from the bank as a freely propagating wave. The conditions of its generation are substantially subcritical. Estimation of the generation parameter $kU_{\max}/\sigma$ (here $U_{\max}$ is the maximum velocity of generating tidal flow, k is the wave number of generated waves, and σ is the tidal frequency) introduced by *Nakamura and Awaji* [2000] and *Nakamura et al.* [2000] to distinguish the unsteady lee-wave regime ($kU_{\max}/\sigma \gg 1$) from the baroclinic tidal regime ($kU_{\max}/\sigma \ll 1$) of generation shows that in our case $kU_{\max}/\sigma = 0.45$ for Wave

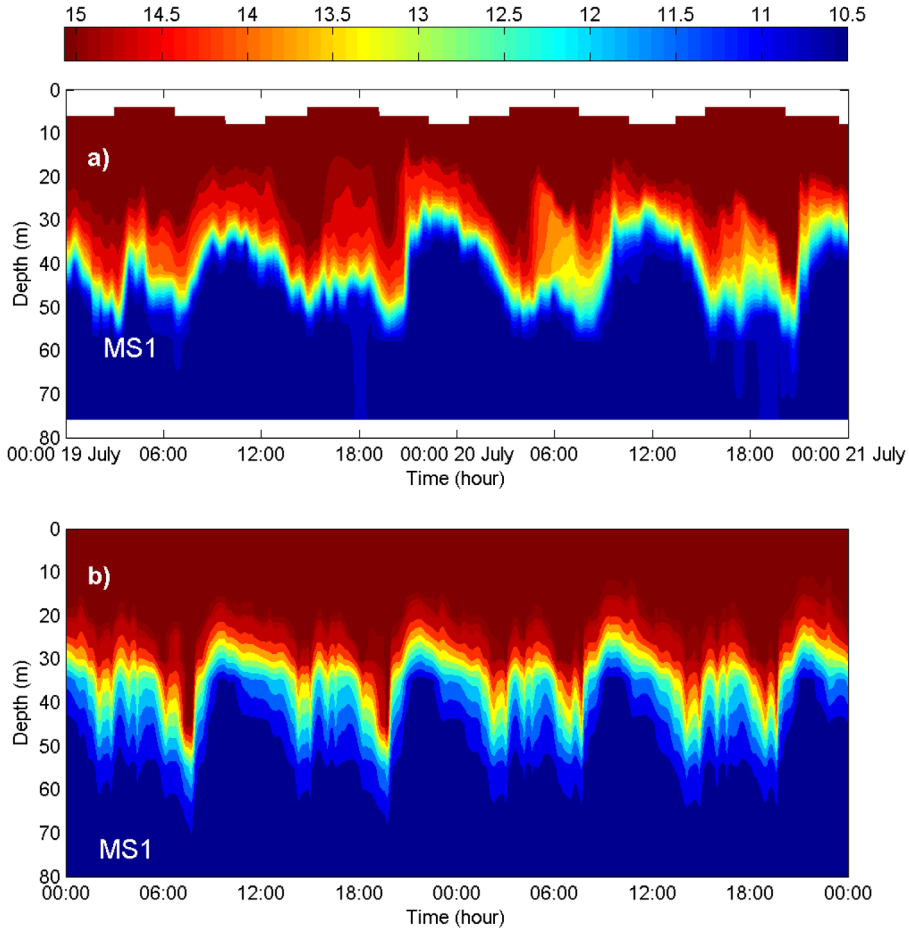

Figure 8. (a) Temperature recorded at mooring MS1 on 19–21 July 2008. (b) Model-predicted temperature at mooring MS1.

3, which belongs to a mixed-tidal-lee wave mechanism of generation (transition between the two). In the mixed regime, the generated waves are not arrested by the flow but freely propagate away from the topography, although they can be accelerated or decelerated at some stages of their evolution, as it is seen in Figure 6a. Wave 3 propagated from the bank, transforming into an undulated first-mode baroclinic bore with an amplitude of ~15 m. The value of the surface velocity gradient *Gr* for Wave 3 was at least 10^{-4} s^{-1} smaller than those for Waves 1 and 2. Wave 3 was generated according to an evolutionary mechanism quite different from the "arrested and released" mechanism that produced Waves 1 and 2.

[33] The qualitative difference between "arrested and released" and "evolutionary" mechanisms can be explained quantitatively in terms of a Froude number analysis. The Froude number was calculated as follows:

$$Fr_i = \vec{U} \cdot \vec{n}/c_i, \quad (1)$$

where $\vec{U}$ is the vector of the velocity of the barotropic tidal current (calculated separately for the homogeneous fluid), $\vec{n}$ is the unit vector normal to the wave front, and c_i is the phase speed of the first or second mode ($i = 1, 2$) obtained from a standard boundary value problem:

$$\frac{d}{dz}\left\{[c_i - U(z)]^2 \frac{d\Phi}{dz}\right\} + N^2(z)\Phi = 0,\ \Phi(0) = \Phi(-H) = 0. \quad (2)$$

Here Φ is the modal structure function.

[34] The Froude numbers were estimated at different moments in time at the positions where the signatures of Waves 1 and 2 are crossed by dashed lines in Figure 6a. Figure 6b shows time dependences of the Froude numbers in red (Wave 1) and blue (Wave 2) lines. The dashed and solid lines in Figure 6b refer to the first mode and the second mode, respectively. Note that the Froude number defined by equation (1) can be a positive or negative number depending on the direction of the tidal current.

[35] Figure 6b shows that the Froude number for the first mode, $|Fr_1|$, is mostly <1, i.e., subcritical; thus, the conditions for the first-mode internal wave generation in the area of Jones Bank are subcritical. As a result, the first-mode Wave 3 is not initially arrested by the tide but freely radiates from the bank and steepens to a solibore (Figure 7).

[36] The large value of the Froude number for the second baroclinic mode, $|Fr_2| > 1$ (for both Waves 1 and 2), results in the wave arrest at the lee side of the bank. During the arrest phase, the wave absorbs energy from the mean flow and grows in amplitude to a large-amplitude wave (Figure 7). The subcritical condition for the first mode and

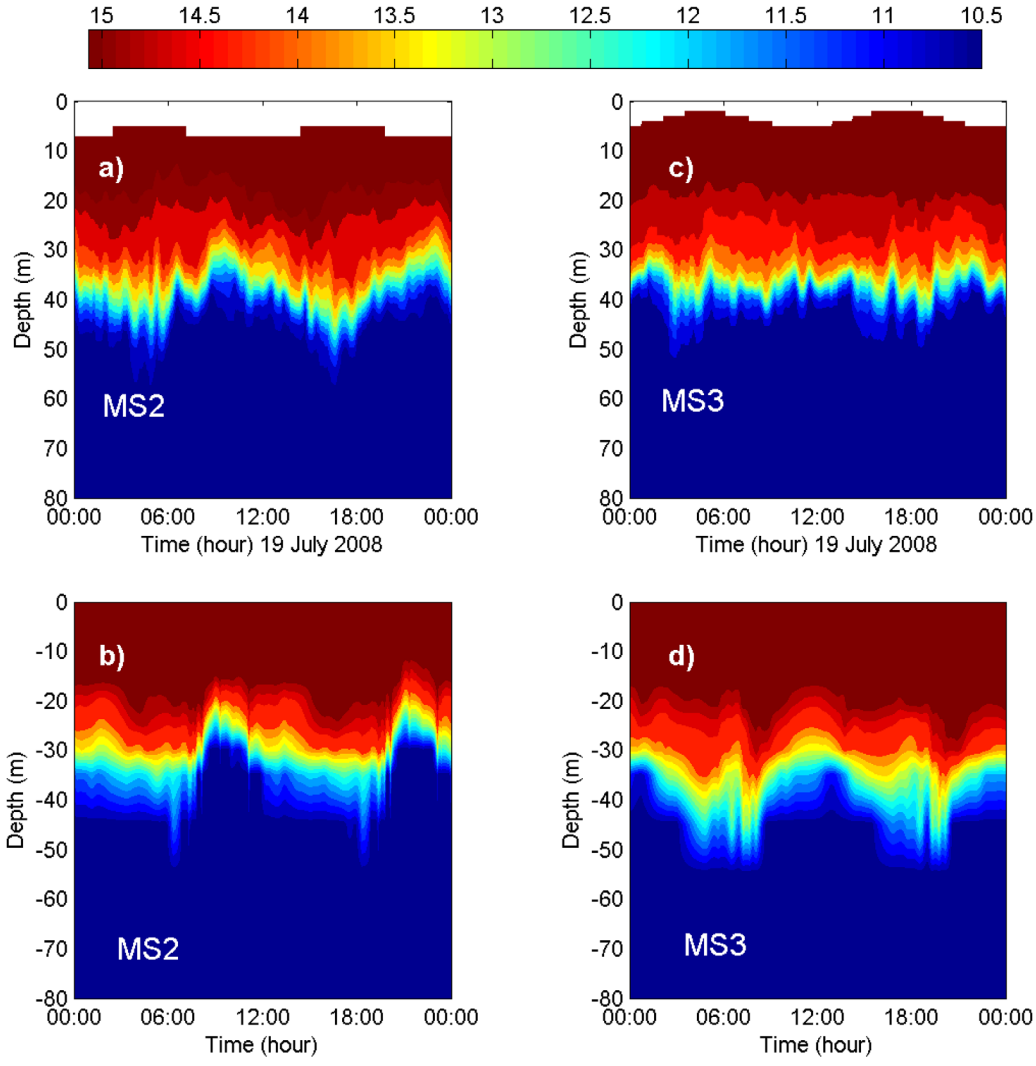

Figure 9. Temperature time series from measurements for moorings (a) MS2 and (c) MS3. Temperature time series from model for moorings (b) MS2 and (d) MS3.

supercritical for the second-mode waves result in their quick spatial separation at their place of generation because the first mode can freely propagate from the place of generation.

4.2. Experiment II: Tidal Forcing and Stationary Current

[37] The hydrographic conditions around Jones Bank in July 2008 gradually changed during the period of field observations. By the time of the next spring tide (the second part of July), a background quasi-stationary current had developed in the area, reaching 0.05 m s^{-1} on 19 July 2008 (see Figure 2). To replicate the hydrological conditions that occurred on 19–21 July 2008, the next series of model runs (Experiment II) was conducted with both tidal forcing and the background current activated in the model. Taking into account the fact that the phase speed of the first-mode waves in the beginning of July was nearly equal to the velocity of the tidal current (VE = 0.4 m^{-1}; VN = 0.3 m^{-1}), this additional relatively weak background flow dramatically changed the regime of their generation. This is seen from the comparative analysis of the observational data collected at moorings and the results of modeling obtained without (Figures 4a, 4c, and 4e) and with (Figures 8a, 9a, and 9c) an extra current.

[38] Two-day temperature records at mooring MS1 and similar model density sampling are shown in Figures 8a and 8b, respectively. Figure 9 shows the temperature at moorings MS2 and MS3 (Figures 9a and 9c) and model temperature records (Figures 9b and 9d). A general, excellent agreement (even in small details) between the model and experimental data sets is evident. There is a clear disparity between results before and after the introduction of an extra background flow; initial results (Figure 4) revealed elements of time series with out-of-phase isothermal displacements, whereas a second series of results (Figures 8 and 9) identifies isothermal displacements to be in phase, which is indicative of the first mode.

[39] Similarly, as was done in section, 4.1, the three-dimensional structure of internal waves was studied using the gradient of horizontal velocities at the free surface (presented in Figure 10). The comparison between surface signatures obtained for 7 July 2008 (Figure 5) and 19 July 2008 (Figure 10) reveals quite different wave positions

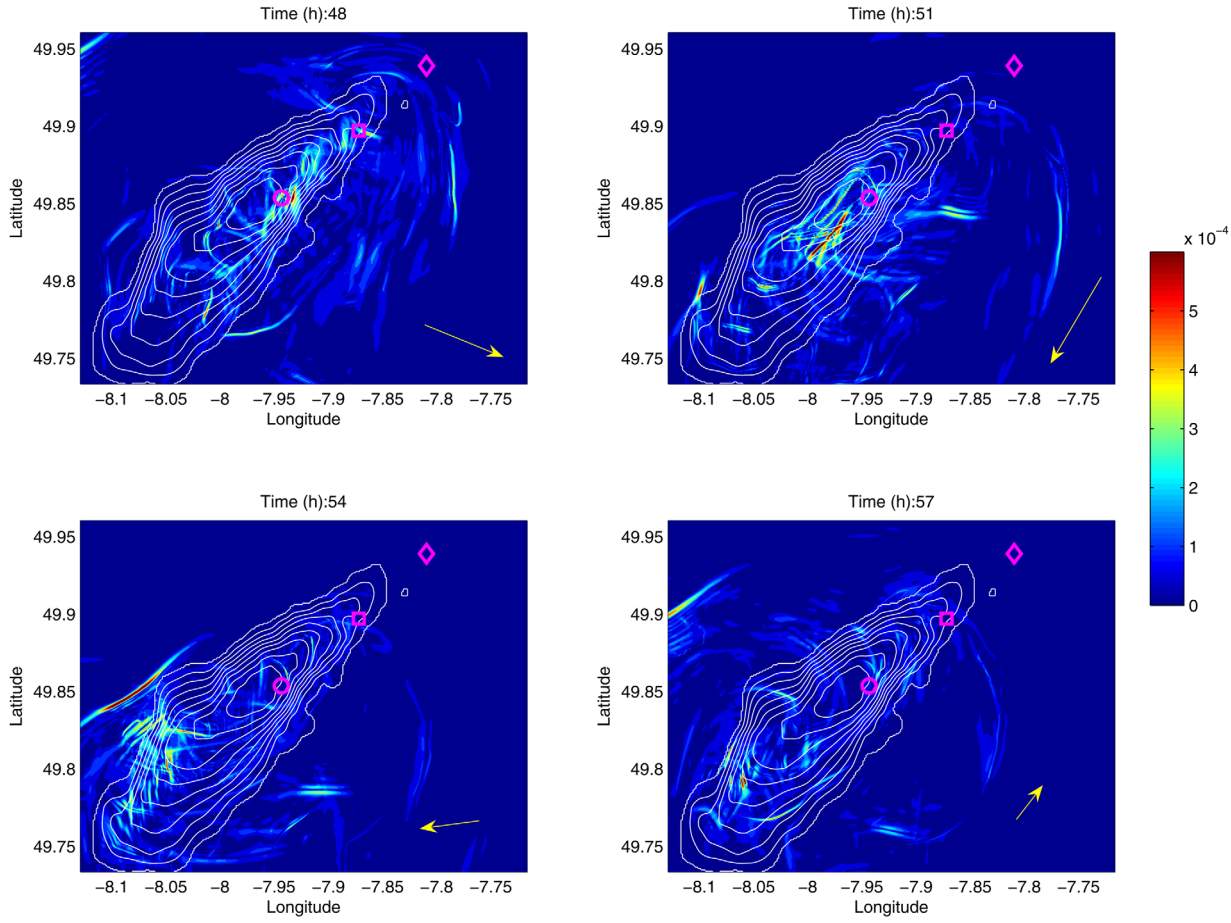

Figure 10. Gradients of horizontal velocity *Gr* (in s^{-1}) on the free surface (light blue and yellow-red colors) at different stages of tidal cycle showing evolution of internal waves radiated from Jones Bank. Yellow arrows show the direction and strength of the tidal current. Positions of moorings are shown by red symbols.

around the bank. This difference between the two experiments indicates that the regime of generation of internal waves in the area of Jones Bank is highly sensitive to the presence of the even weak background currents.

[40] A more accurate analysis, based on the joint investigation of particular wave signature and corresponding vertical cross section (as it was done in section 4.1), allows us to specify the detail characteristics of the radiated waves. Figure 11a shows a summary illustration of hourly signature of the three strongest wave groups generated over the bank. The leading Waves 1, 2, and 3 are presented in red, blue, and green colors, respectively. The dashed lines of the respective colors indicate the route of wave propagation. The instant values of the Froude numbers estimated for the leading wave of every packet are shown in Figure 11b. Figure 12 shows vertical density cross sections for Waves 1, 2, and 3 at different moments in time.

[41] It is clear that Wave 1, generated at the northeastern flank of the bank (Figure 11a), is arrested there (see wave signature for $t = 48$ h and $t = 49$ h). The cophase displacements of isopycnals shown in the top row of Figure 12 specify this wave as first mode with vertical displacement of ~30 m. Wave 1 is arrested for 2 h and is released when the tidal flow slackened and changed direction. After its release, Wave 1 propagates to the NW, transforming into a baroclinic bore that ultimately disintegrates into a first-mode wave packet, with the amplitudes of the leading wave of ~20 m.

[42] Wave 2 (blue signatures in Figure 11a) is generated to the south of the location where Wave 1 was formed. It initially resembles a hydraulic jump with an amplitude of ~30 m (middle row in Figure 12). The wave is arrested at the lee side of the bank topography for 2 h and, similarly to Wave 1, transforms into a bore and disintegrates into a packet of first-mode solitary waves with an amplitude of 20 m.

[43] Green signatures depicted in Figure 11 show the evolution of Wave 3. It is clear that during a 2 h time span ($t = 49$–51 h) Wave 3 moves in the opposite direction to Wave 1. The vertical cross sections of the wave shown in Figure 12 clearly indicate that Wave 3 is second mode. The inset in Figure 11a represents the tidal diagram where the direction and value of the current are shown by arrows. The increase of eastward velocity toward the east due to background current results in advection of the second mode from its place of generation.

[44] Such a radical change in the wavefield dynamics, where the second-mode large-amplitude internal waves observed in Figures 6a and 7 were replaced by the large-amplitude first-mode internal waves shown in Figures 11a and 12 can be explained in terms of the Froude number analysis. The Froude numbers were calculated using equation (1) for every particular wave for the position where dashed lines

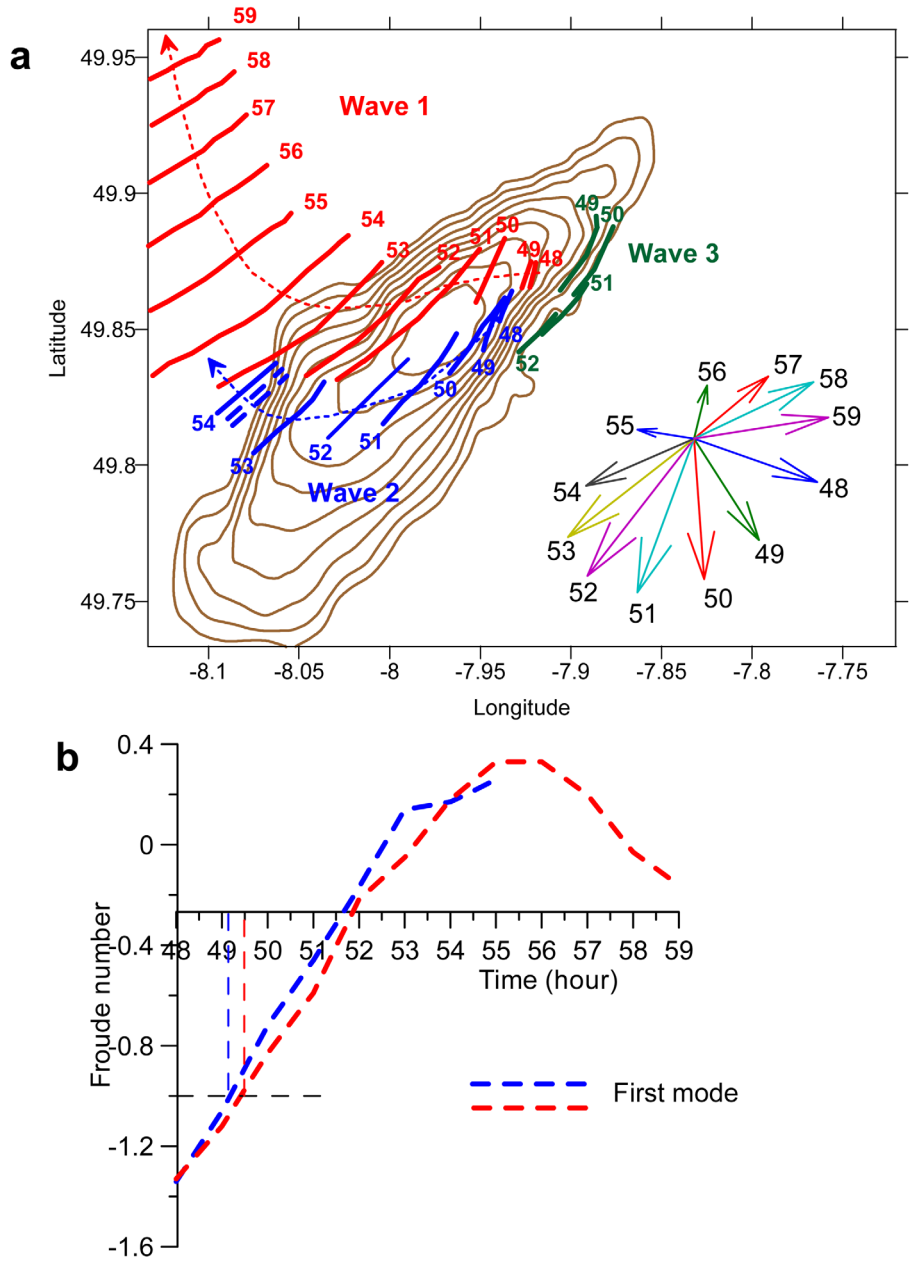

Figure 11. (a) Surface signature of internal waves that were generated at different moments of tidal cycle. Positions of only the strongest wave packets are presented with 1 h interval. Direction and strength of the tidal currents are shown by a tidal diagram in the bottom right. (b) The Froude number calculated for Waves 1 and 2 in the positions where their centers were at every particular moment of time (along dashed lines). The Froude number for the second mode Wave 3 calculated for the time span 47–51 h was >3.

cross the wave fronts. Figure 11b shows that the Froude number becomes supercritical for the first baroclinic mode because of the extra flow to the south. With this modification, the tidal diagram became asymmetric with strong predominance of the southeastern components (compare the tidal diagrams in Figures 6 and 11). This creates favorable conditions for the blocking of the first baroclinic mode. Thus, the first-mode Waves 1 and 2 are arrested for more than 1 h and absorb energy from the tidal flow. When the tidal flow slackens and changes its direction, both waves are released and freely radiate over and away from the bank.

[45] For the second-mode waves, the extra background current increases the maximum Froude number $|Fr_2|$ to the value of 3. In a substantially supercritical regime, the second and higher modes do not have any chance to grow and build up their amplitude because they are just washed away from the generation site by a strong, supercritical current.

5. Summary and Conclusions

[46] The idea of this paper was to reproduce numerically the internal wavefields generated by a stratified tidal flow

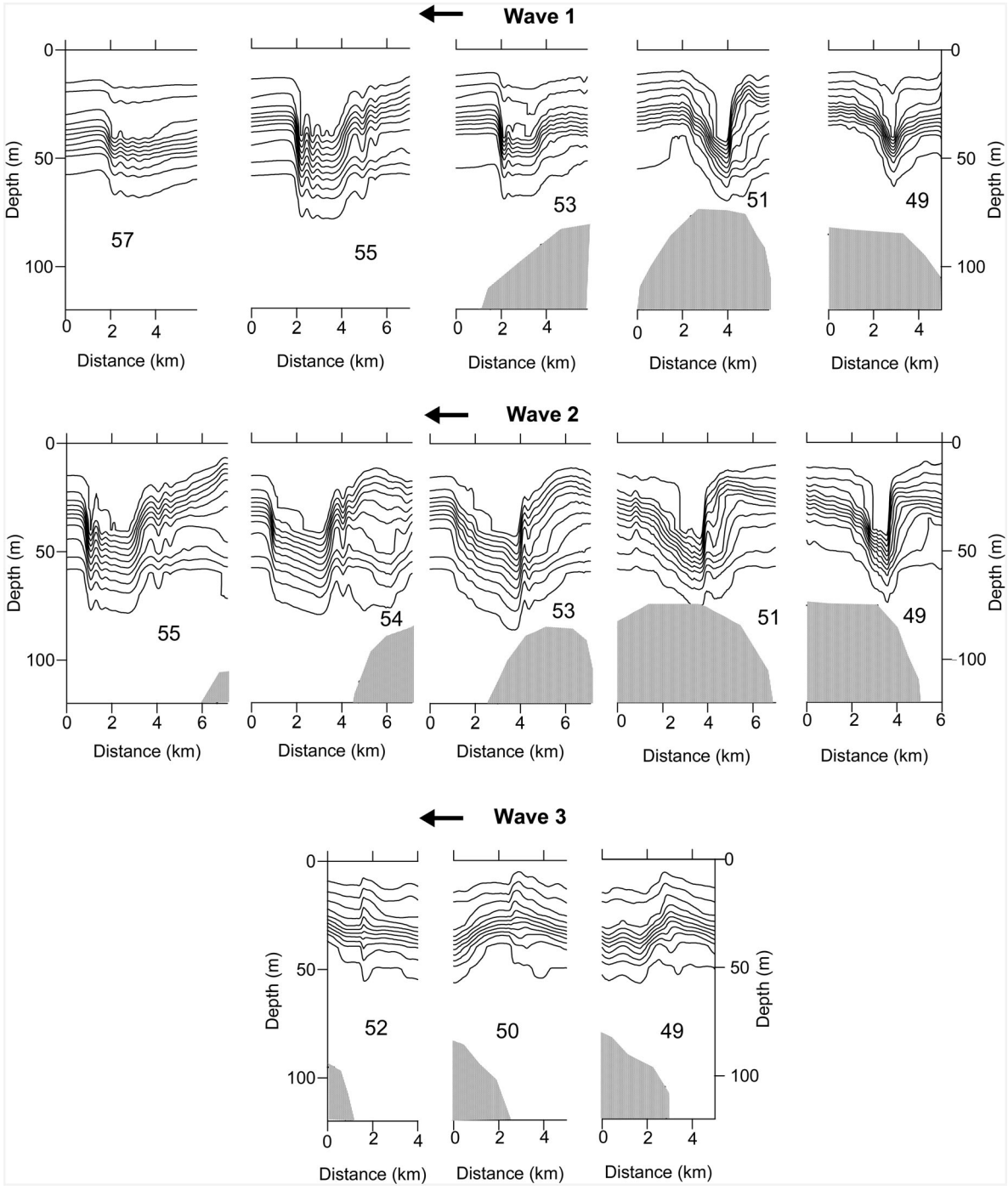

Figure 12. Cross sections along the blue and red dashed lines in Figure 10a. The line interval is equal to 0.1 kg m^{-3} starting with $\sigma_t = 26.1$ kg m^{-3} at the shallowest isoline. Numbers in the middle of every plot depict the moment of tidal cycle in hours.

interacting with Jones Bank (the Celtic Sea). The MITgcm model was initialized and validated against the observational data collected at three moorings, MS1, MS2, and MS3, deployed in the area during the field experiment conducted in July 2008 [*Palmer et al.*, 2013]. Analysis of a time series recorded at mooring MS1 located near the bank's crest has shown that the hydrographic conditions in the experimental domain varied over the observational period. Relatively weak background currents recorded in the beginning of the experiment (on 7 July 2008) gradually turned to a moderate (0.05 m s^{-1}) southeasterly directed background flow observed on 20–22 July 2008. Both scenarios, i.e., with only tidal forcing included in the model and in combination with the background current, were reproduced numerically. An additional stationary current in the second series of experiments was initiated in the model by an extra term added to the RHS of the momentum balance equations. The comparison analysis of the in situ data and the model output revealed their

coincidence, which suggests that the model reproduces the real internal wavefield generated over Jones Bank.

[47] An interesting finding from the present study is the identification of two different scenarios of internal wave generation that occurred over Jones Bank during the cruise campaign. In the first series of numerical experiments with only tidal forcing activated in the code (conditions of the beginning of the observations), the tidal flow was subcritical (in terms of the Froude number) for the first baroclinic mode but supercritical for the second mode. As a result, the first-mode waves were generated and freely radiated from the bank, transforming into a dissipative baroclinic bore. As distinct from that, the second-mode waves were arrested at the lee side of the bank for quite a long period of time (3 h), and grew in amplitude (up to 35 m). They were released and propagated off the bank as a series of second-mode internal solitary waves when the tidal flow changed its direction.

[48] In the second series of numerical experiments, an additional stationary forcing was activated in the model to reproduce an extra background current which was observed in the area at the next spring tide. With this extra current, the flow over the bank becomes supercritical to the first baroclinic mode, and those waves were arrested at the lee side of the topography for almost 2 h, where they built up their amplitude to almost 40 m in the vertical.

[49] After release, the first-mode wave radiated from the bank as an undulating bore gradually transforming into a packet of solitary internal waves. Under such conditions, the flow became substantially supercritical for the second-mode perturbations; thus, they were permanently washed away from the generation site without any substantial amplification.

[50] The formulated conclusion that the place of wave generation is very sensitive to the background currents is in agreement with the measurements of *Moum and Nash* [2000] conducted in April 1998 near Stonewall Bank (Newport, Oregon). It was found there that the measurements made at the very same location 2 days apart showed no obvious signs of hydraulically controlled flow (Froude number exceeds one) which was observed 2 days earlier.

[51] As seen in Figures 6 and 11, at the very beginning of the tidal cycle the along-front length of the initially arrested lee waves did not exceed 200 m; however, after 3–4 h the length of the wave fronts increased 5–10 times. Such characteristics of generated waves are consistent with the observations by *Dewey et al*. [2005], who examined the interaction of stratified tidal currents over a bump in the Race Rocks area (British Columbia). They reported that during the slackening ebb tide, the "released" lee wave was not observed. They explained this as a possible consequence of its limited spatial size, although backscatter satellite imagery of the region consistently shows internal wave packets radiating from the bank.

[52] The numerical experiments reported here provide two salutary lessons to analysts of in situ observations in the vicinity of topographic features in stratified shelf seas. First, very small changes in mean flows can radically alter the response of the stratified fluid to tidal forcing. Second, a rich multimodal and 3-D structure to the high-frequency internal wavefield might reasonably be expected, even when topographic geometry is relatively simple, presenting considerable experimental design and interpretational challenges to the observer.

[53] **Acknowledgment.** This work was initiated during the start of Natural Environment Research Council grant FASTNEt. NE/I030224/1. We thank the officers and crew of the RRS "James Cook" and staff at NMFSS and NOC for their assistance in collecting the presented observational data which was funded under the UK Natural Environment Research Council Ocean2025 strategic marine science programme.

References

Brickman, D., and J. W. Loeder (1993), Energetics of internal tide on northern Georges Bank, *J. Phys. Oceanogr.*, *23*, 409–424.

Carter, G. S., M. C. Gregg, and M. A. Merrifield (2006), Flow and mixing around small seamount on Kaena Ridge, Hawaii, *J. Phys. Oceanogr.*, *36*, 1036–1052.

Dewey, R., D. Richmond, and C. Garrett (2005), Stratified tidal flow over a bump, *J. Phys. Oceanogr.*, *35*, 1911–1927.

Egbert, G. D., and S. Y. Erofeeva (2002), Efficient inverse modeling of barotropic ocean tides, *J. Atmos. Oceanic Technol.*, *19*(2), 183–204.

Farmer, D., and L. Armi (1999), The generation and trapping of solitary waves over topography, *Science*, *283*, 188–190.

Garrett, C., and E. Kunze (2007), Internal tide generation in the deep ocean, *Annu. Rev. Fluid Mech.*, *207*(39), 57–87.

Hibiya, T. (1988), The generation of internal waves by tidal flow over Stellwagen Bank, *J. Geophys. Res.*, *93*(2), 533–542.

Holloway, P., and M. Merrifield (1999), Internal tide generation by seamounts, ridges and islands, *J. Geophys. Res.*, *104*(C11), 25,937–25,951.

Inall, M. E., D. Aleynik, T. Boyd, M. R. Palmer, and J. Sharples (2011), Internal tide coherence and decay over wide shelf sea, *Geophys. Res. Lett.*, *38*, L23607, doi:10.1029/2011GL049943.

Johnston, T., and M. Merrifield (2003), Internal tide scattering at seamounts, ridges and islands, *J. Geophys. Res.*, *108*(C6), 3180, doi:10.1029/2002JC001528.

Klymak, J. M., R. Pinkel, and L. Rainville (2008), Direct breaking of the internal tide near topography: Kaena Ridge, Hawaii, *J. Phys. Oceanogr.*, *38*, 380–399.

Klymak, J. M., S. Legg, and R. Pinkel (2010), A simple parameterization of turbulent tidal mixing near supercritical topography, *J. Phys. Oceanogr.*, *40*, 2059–2073.

Marshall, J., A. Adcroft, C. Hill, L. Perelman, and C. Heisey (1997), A finite-volume, incompressible Navier-Stokes model for studies of the ocean on the parallel computers, *J. Geophys. Res.*, *102*(C3), 5753–5766.

Moum, J. N., and J. D. Nash (2000), Topographically induced drag and mixing at a small bank on the continental shelf, *J. Phys. Oceanogr.*, *30*, 2049–2054.

Munroe, J. R., and K. G. Lamb (2005), Topographic amplitude dependence of internal wave generation by tidal forcing over idealized three-dimensional topography, *J. Geophys. Res.*, *110*, C02001, doi:10.1029/2004JC002537.

Nakamura, T., and T. Awaji (2000), The growth mechanism for topographic internal waves generated by an oscillatory flow, *J. Phys. Oceanogr.*, *31*, 2511–2524.

Nakamura, T., T. Awaji, T. Hatayama, K. Akimoto, T. Takizawa, T. Koho, Y. Kawasaki, and M. Fukasava (2000), The generation of large-amplitude unsteady lee waves by subinertial tidal flow: A possible vertical mixing mechanism in the Kuril Straits, *J. Phys. Oceanogr.*, *30*, 1601–1621.

Nash, J. D., and J. N. Moum (2001), Internal hydraulic flow on the continental shelf: High drag states over a small bank, *J. Geophys. Res.*, *106*, 4593–4611.

Pacanowski, R. C., and S. G. H. Philander (1981), Parameterisation of vertical mixing in numerical models of tropical oceans, *J. Phys. Oceanogr.*, *11*, 1443–1451.

Palmer, M. R., M. Inall, and J. Sharples (2013), The physical oceanography of Jones Bank: A mixing hotspot in the Celtic Sea, *Prog. Oceanogr.*, doi: 10.1016/j.pocean.2013.06.009.

Stashchuk, N., and V. Vlasenko (2005), Topographic generation of internal waves by nonlinear superposition of tidal harmonics, *Deep Sea Res., Part I*, *52*, 605–620.

Vlasenko, V., N. Stashchuk, and K. Hutter (2005), *Baroclinic Tides*, 351 pp., Cambridge Univ. Press, Cambridge.